

Influence of Post-Treatment Temperature on the Stability and Swelling Behavior of Casein Microparticles

Md Asaduzzaman and Ronald Gebhardt*

This study investigates the influence of exposure time and post-treatment temperature on the stability and swelling of casein microparticles prepared by depletion flocculation and film drying. Stability experiments with sodium dodecyl sulfate at 20 °C show that particles become more stable with higher post-treatment temperature and longer exposure times. The two-step decrease in decay rates in each case indicates a stable intermediate state structurally different from untreated and more strongly treated microparticles. The swelling curves of microparticles also show differences in three temperature ranges at 120 min exposure times each, which is analyzed with dynamic swelling models. At temperatures $T \leq 50$ °C, the casein microparticles swell and decompose in a typical two-step process. For post-treatments in the temperature range between $T = 60$ and 70 °C, the swelling curves change their shape toward limited swelling to an equilibrium swelling value. The swelling curves of microparticles treated with temperatures at 80 and 90 °C show a typical overshooting, which can be analyzed with an adapted parallel swelling model and attributed to an elastic network of newly formed bonds.

before use is essential to meet microbiological safety and hygienic requirements.^[8,9] However, the heat resistance of most of these materials is insufficient,^[10] and proteins in particular exhibit many structural and functional changes that should be investigated in advance. The casein conformation, however, is open and flexible (rheomorphic) and does not show heat-induced changes to a more disordered structure.^[11,12] Nevertheless, heat-induced changes occur, related to the self-assembling of the caseins to higher aggregated structures, which will be described below. In milk, four different caseins (α_{S1} -, α_{S2} -, β -, and κ -casein) form spherical aggregates together with colloidal calcium phosphate. The number distribution of these so-called casein micelles exhibits a maximum at a radius of 50–100 nm.^[13] An understanding of the stability and swelling behavior of the carrier material

1. Introduction


Caseins are the main protein component in milk and a natural nanocarrier for highly insoluble calcium phosphate and small bioactive molecules or larger macromolecules.^[1] Important technological applications of nanostructures engineered from casein are encapsulation systems for bioactive substances, such as curcumin and vitamins in foods, drugs in cancer therapy, or antibacterial agents in animal feeds.^[2–5]

With casein, a biocompatible, biodegradable, and biore-sorbable material can be used and synthetic additives are avoided.^[6,7] Generally, heat treatment of the bio-based sample

casein is necessary for its future use as a delivery platform. Internally, casein micelles are stabilized by two important molecular interactions related to the flexible structure of casein monomers, closely resembling block copolymers.^[14] The hydrophilic blocks contain phosphoserine clusters that can combine with colloidal calcium phosphate, and the hydrophobic blocks form casein–casein interactions. The latter interactions significantly contribute to the overall stability, as demonstrated by nanomechanical studies.^[15] High-pressure measurements have shown that hydrophobic interactions increasingly stabilize casein micelles at higher temperatures and that a maximum effect is reached at $T = 80$ °C.^[16] Stability studies with sodium dodecyl sulfate (SDS) have shown that the surfactant molecules interact with caseins mainly via hydrophobic bonds.^[17] In addition, a surface layer of κ -casein exerts steric repulsion and is essential for the colloidal stability of casein micelles.^[18]

The Flory–Rehner theory explains the swelling state of gel structures at equilibrium in terms of the free energy of mixing, the elastic deformation of the network, and ionic contributions.^[19] In a good solvent, the system gains mixing and configurational entropy and loses the latter when the stretching of the polymer network occurs due to swelling.^[20] For this reason, hydrogels made of hydrophilic polymers with low density of crosslinks in the network and high charge density in the polymer chains swell particularly strongly.^[21] Also, studies on acrylamide gels have shown that the swelling rate decreases with increasing cross-linking concentration. As a consequence of more

M. Asaduzzaman, R. Gebhardt
RWTH Aachen University
Chair of Soft Matter Process Engineering (AVT.SMP)
Forckenbeckstraße 51, 52074 Aachen, Germany
E-mail: ronald.gebhardt@avt.rwth-aachen.de

 The ORCID identification number(s) for the author(s) of this article can be found under <https://doi.org/10.1002/mame.202200661>

© 2023 The Authors. Macromolecular Materials and Engineering published by Wiley-VCH GmbH. This is an open access article under the terms of the Creative Commons Attribution License, which permits use, distribution and reproduction in any medium, provided the original work is properly cited.

DOI: 10.1002/mame.202200661

cross-links in the gel, smaller equilibrium swelling percentages result.^[22,23] Casein micelles can be considered as a sponge-like structure,^[1,24,25] being highly hydrated with about 3.3 g of water per g dry mass. Of this amount of water, 15% each is either firmly attached to the κ -casein surface layer or other caseins, while the remaining 55–60% is trapped in channels or cavities within the structure.^[26]

Casein micelles lose their colloidal stability, aggregate, and form a gel when the steric repulsion of the κ -casein surface layer is decreased, e.g., after acidification or enzymatic hydrolysis.^[27] If the pH is lowered to below 6.4, gelation of casein micelles can also be induced by heating to temperatures below 90 °C, with the critical temperature decreasing with falling pH and increasing casein concentration.^[28] Instead, we developed a gentle aggregation process at neutral pH and room temperature where volume exclusion of added pectin leads to aggregation of casein micelles via depletion flocculation. These casein aggregates are then stabilized by film drying, isolated from the pectin matrix by enzymatic degradation, and resuspended in any buffer.^[29,30] The resulting casein microparticles (CMPs) are spherical objects with sizes between 5 and 50 μm . They have an internal structure consisting of a network of casein building blocks with a size of a few μm interspersed with water channels of similar size.^[31] By changing the milieu conditions or process parameters during the manufacturing process, we obtained CMPs with different structures and properties as described in detail below. In particular, different stabilities and swelling behaviors of the particles can be adjusted, which are important functional properties given a future application as carriers with immediate and controlled release of encapsulated bioactive substances. The stability of CMPs can be tested by analyzing their decomposition after adding sodium dodecyl sulfate.^[32] Our recent studies have shown that CMPs prepared under standard conditions decay completely mono-exponentially, suggesting that the microparticles are held together mainly by hydrophobic interactions. CMPs prepared under standard conditions swell and disintegrate under basic pH conditions but remain stable in acidic media (even in 1 N HCl) and in ultrapure water.^[33] Swelling occurs more rapidly the higher the pH, lasting hours at pH 8, minutes at pH 11, and only a few seconds at pH 14. Swelling always proceeds in two steps. The corresponding data can be analyzed with a dynamic model approach, which in the past has also been used to simulate complex processes such as parallel crystallization and aggregation or permeation of drugs during particle dissolution and membrane diffusion.^[34,35] Pre- and post-treatment strategies can be applied to CMPs to obtain tailored functional properties. We have demonstrated that adding citrate at the beginning of the production process chelates calcium from the colloidal calcium clusters of casein micelles, resulting in a more negative charge on the phosphoserine clusters of caseins. This, in turn, results in enhanced swelling of the CMPs at pH 8 due to increased electrostatic repulsion and water binding, whereas at pH 3, the particles remain stable due to protonation.^[36] At the end of the swelling process, the microparticles disintegrate completely, which may be desirable for applications as a carrier material with immediate release of the bioactive substance. However, to regulate the release via swelling, it is preferable to have additional structural stability of the microparticles, for instance, by enzymatic cross-linking by transglutaminase, TGase.^[20] Our studies showed that CMPs without cross-

links completely decomposed after adding SDS, while CMPs treated with TGase remained stable due to additionally introduced isopeptide bonds.^[37] The stabilization also results in CMPs expanding to an equilibrium state rather than entirely decomposing during swelling. As a new feature in the swelling curves, overshooting occurs during rapid swelling at pH 14, which is more pronounced the longer the treatment time with the crosslinking enzyme. A parallel model approach, which assumes that a cross-linked casein fraction restricts the swelling of noncross-linked caseins in the core by forming an elastic network, can be used to describe all swelling curves of CMPs subsequently cross-linked with TGase.^[37] Complex swelling kinetics with overshoot has been described previously for other polymer systems, with the effect attributed to the ionic contribution.^[38,39,40] Subsequent heating could also affect the stability and swelling of supramolecular casein structures, such as CMPs, which are held together largely by temperature-dependent hydrophobic interactions.^[41] In the temperature range up to 40 °C, the amount of soluble casein – mainly β -casein –, hydration, and apparent voluminosity of casein micelles decreases at a higher temperature.^[42] A 1H-NMR spectroscopy study showed that in the temperature range above 70 °C the rigid structure of the casein micelles started to melt, which can be attributed to the increased mobility of the caseins.^[43] At temperatures $T > 70$ °C and neutral pH, the thiol-disulfide exchange interaction between casein and whey protein plays a significant role in the heat stability of casein micelles in natural milk.^[9,44]

The study aimed to investigate the effects of temperature post-treatment on the stability and swelling properties of CMPs. For this purpose, CMPs were heat-treated in a temperature range from 40 to 90 °C for periods between 30 and 180 min. Based on the results of previous studies, we hypothesized that heat-induced changes in the structure and interactions of casein micelles might also affect the stability and swelling properties of CMPs.

2. Experimental Section

2.1. Materials

Potassium hydroxide (>90%), sodium hydroxide (1 M), hydrochloric acid (1 M), and pectinase from *Aspergillus niger* were purchased from Merck (Merck, Darmstadt, Germany). Casein micelle concentrate powder MC80 was delivered by Milei GmbH Germany, and highly methylated citrus pectin (CU 201, DE° >70%) was kindly provided by Herbstreith & Fox (Herbstreith & Fox GmbH & Co. KG, Neuenbürg, Germany). BisTris methane, calcium chloride, Sodium dodecyl sulfate, and all salts for simulated milk ultrafiltrate (SMUF) preparation were obtained from VWR, Darmstadt, Germany. For preparing the solution, Milli-Q water was obtained from the lab water purification system (Simplicity UV System, Merck, Darmstadt, Germany).

2.2. Preparation of Working Solutions

The working buffer solution (50 mM BisTris, 10 mM CaCl_2) was prepared by dissolving 10.462 g BisTris and 1.11 g CaCl_2 in

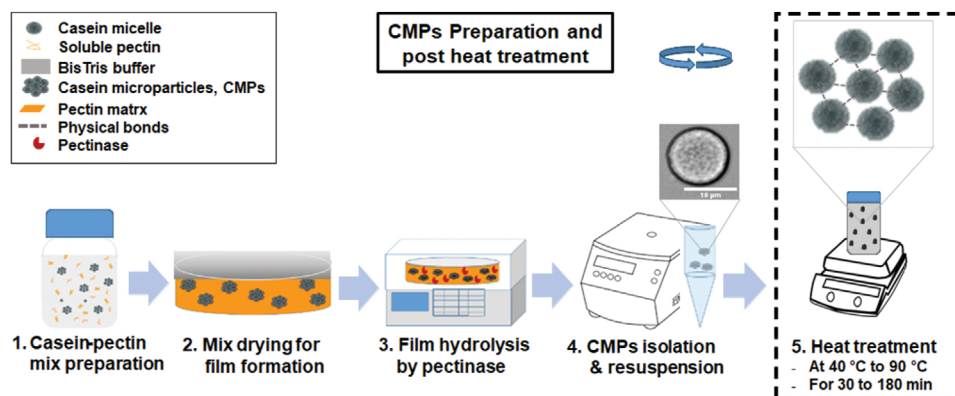


Figure 1. Process steps required to produce CMPs at $T = 20\text{ }^{\circ}\text{C}$ and under neutral pH conditions. The post-treatment step, which is investigated in detail in this study, is highlighted.

1000 mL milli-Q water. After complete dissolution, the pH of the solution was adjusted to pH 6.8 using the required amount of 1 M HCl solution.

SMUF buffer was prepared following the preparation method described by Dümpler et al.^[45] Briefly, all salts were dissolved in milli-Q water step by step with continued stirring. Finally, pH was adjusted at 6.7 by adding 1 M KOH solution.

Pectin solution (2%) was prepared by adding 2 g citrus pectin in 98 g BisTris buffer solution. The mixture was vigorously stirred at $80\text{ }^{\circ}\text{C}$ for 3 h to completely dissolve the pectin. After that, the pectin solution was cooled at $20\text{ }^{\circ}\text{C}$, and the pH was adjusted to 6.8 using the required amount of 1 M NaOH solution.

Casein dispersion was prepared by adding 5 g casein powder in 45 g SMUF solution to achieve the final concentration of 7.36% casein. The casein solution was stirred for 1 h at room temperature, then 4 h at $4\text{ }^{\circ}\text{C}$ followed by another hour at $37\text{ }^{\circ}\text{C}$, each at 200 rpm. The pH value of the casein solution was 6.7.

For film hydrolysis, a working pectinase solution was prepared by adding 0.47 mL pectinase from *Aspergillus niger* to 10 g buffer to obtain enzyme activity $\approx 36\text{ units mL}^{-1}$.

2.3. Preparation of CMPs

The CMPs production process was based on the principles of depletion flocculation interaction between casein micelles and pectin.^[46,47] The specific preparation steps are summarized in **Figure 1** according to a protocol described by Gebhardt et al.^[37] Briefly, the casein, pectin, and BisTris buffer solution were appropriately mixed to end up with the solution having casein and pectin concentrations of 3.0% and 0.3%, respectively. To prepare the casein-pectin film, 3.9 g mixed solution was evenly spread on a glass petri dish ($\varnothing 70\text{ mm}$) and dried under a controlled lab environment ($T = 22\text{ }^{\circ}\text{C}$, RH 45%) for 16 h. The casein aggregates formed during the mixing step were deformable but compressed and solidified during the drying process of the film. For the enzymatic hydrolysis of film, 10 mL of pectinase solution (37 unit mL^{-1} in buffer solution) was added to the petri dish. The hydrolysis was performed in a ThermoMixer (Eppendorf, Eppendorf AG, Hamburg, Germany) by continuous shaking (160 rpm) at $47\text{ }^{\circ}\text{C}$ for 2 h. After hydrolysis, the supernatant solution was collected

and centrifuged (at $T = 22\text{ }^{\circ}\text{C}$ and 1500 RCF for 10 min) to isolate the microparticles. The isolated CMPs were then resuspended in BisTris buffer solution for further use. To study the effect of temperature post-treatment, a portion of the CMPs solution (0.15 g L^{-1}) was then heated at different temperatures ($T = 40\text{ to }90\text{ }^{\circ}\text{C}$). For each temperature, samples were heated for 30, 60, 120, and 180 min and immediately cooled down by placing them in ice water and stored at $T = 4\text{ }^{\circ}\text{C}$ for further analysis.

2.4. Stability Experiments

The stability of the CMPs was investigated following the turbidity of the CMPs solution according to the protocol described by Asaduzzaman et al.^[36] An aliquot of 1.5 mL CMPs dispersion was transferred in a semimicro cuvette (Eppendorf AG, Germany) and measured using a Lambda 365 UV/VIS spectrometer (PerkinElmer, USA). The turbidity of the sample was recorded for 900 s at a wavelength of 600 nm. The turbidity of each sample was measured with or without adding 40 μL SDS solution (520 mM in water) to CMPs dispersion. All samples were measured in duplicate.

2.5. Swelling Experiments

The swelling behavior of CMP was monitored by applying exchange media (ultrapure water, pH 11) in a sieve cell according to the protocol developed by Schulte et al.^[33] The microfluidic sieve cell was filled with CMPs dispersion (in BisTris buffer, pH 6.8) and placed on the stage of an inverted microscope (Leica DMIL LED, Leica Microsystems, GmbH, Wetzlar, Germany). The cell was allowed to stand for 5 min so the CMPs could settle in the sieve holes. The microscope was equipped with a Basler camera (Basler AG, Ahrensburg, Germany) for video recording. A syringe pump (PHD ULTRA Harvard Apparatus, MA) was connected to the swelling cell to deliver the exchange buffer at a flow rate of 0.05 mL min^{-1} . After activation of the syringe pump, the swelling process of the single microparticle trapped in the sieve holes was monitored for 2 h. The video was recorded with the speed of 2 frames s^{-1} using the Basler camera. PyCharm (version

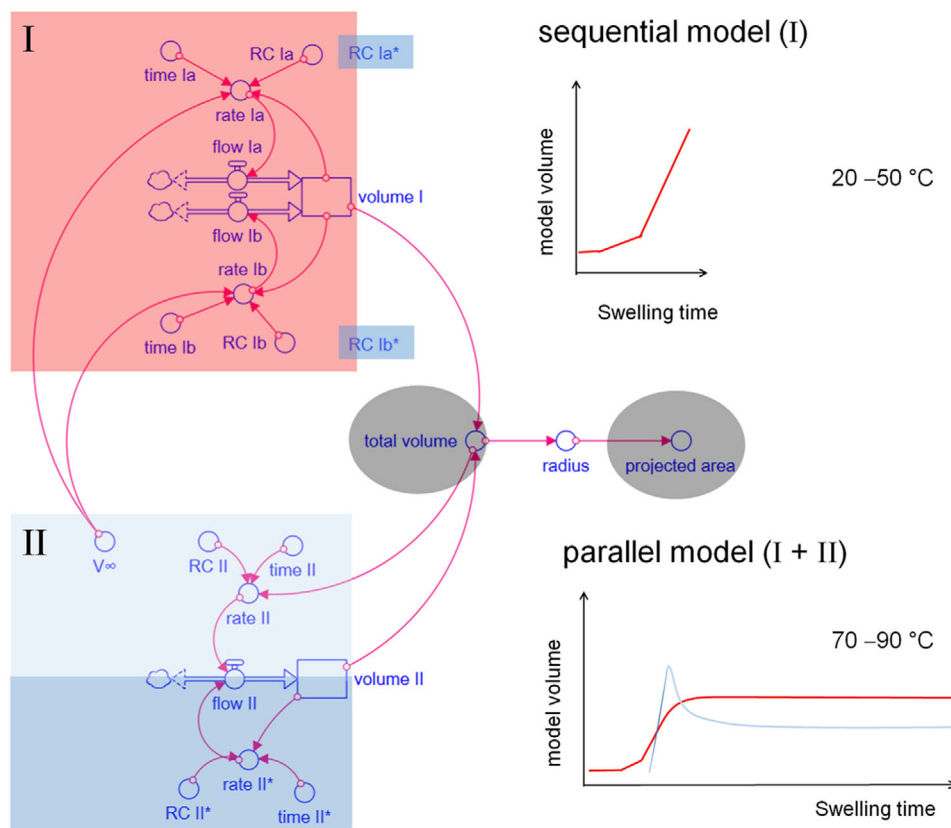


Figure 2. Overview of dynamic STELLA models used to simulate the swelling kinetics. Top: Sequential model according to Schulte et al. for CMPs post-treated at low temperatures.^[33] Bottom: Parallel model modified after Gebhardt et al. for medium and high temperature treatments.^[37]

2021.1.3, JetBrains, Czech) script was used to extract the image frames from the videos. ImageJ software (NIH, USA) was used to calculate the area of the CMPs. At least two repeated measurements were performed for each sample.

2.6. Dynamic Swelling Models

Dynamic models for simulating the swelling kinetics of CMPs were developed using Stella 1.6 software (iseesystems.com, Lebanon, NH). The sequential swelling model was used for the temperature range between $T = 20\text{--}50\text{ }^{\circ}\text{C}$ and a post-treatment time of 120 min.^[33] This swelling model (labeled with I highlighted in red in **Figure 2**) considers CMPs as a reservoir (volume I) with a filling level that can change by two volume flows. Both inflows (flow Ia and flow Ib) depend on the current volume of the reservoir and on rate coefficients (RC Ia and RC Ib) activated by step functions $\sigma(t)$ with characteristic times Ia and Ib, respectively. The rate of change of volume I, which in the sequential model also corresponds to the total volume, is thus given by

$$\frac{d \text{volume}_t}{dt} = \sum_{i=a,b} \text{RC } I_i \cdot \sigma_t^i \cdot \text{volume}_t \quad (1)$$

with

$$\sigma(t) = \begin{cases} 0 & \text{for } t < \text{time } I_i \\ 1 & \text{for } t \geq \text{time } I_i \end{cases} \quad (2)$$

The parallel model approach (I + II in **Figure 2**) assumes that there are two types of caseins within the CMPs, to which volumes I and II are assigned. The noncross-linked casein portion is hydrated and swells in two steps according to the sequential model approach mentioned above. However, the increase of volume I is now limited because of the cross-linked casein fraction, in contrast to the pure sequential swelling model. It was accounted for this by introducing the maximum swelling degree V_{∞} , and second-order swelling kinetics originally used to describe the swelling of gelatin and cellulose in an aqueous medium^[48] but also successfully used recently to simulate swelling kinetics of casein fibers, and CMPs treated with TGase.^[40,37] As a result, the rate coefficients of the swelling steps are no longer comparable and are now denoted as RC Ia* and RC Ib*. The rate of volume change for volume I within the parallel swelling model is

$$\frac{d \text{volume } I_t}{dt} = \sum_{i=a,b} \text{RCI}_i^* \cdot \sigma_t^i \cdot (V_{\infty} - \text{volume } I_t)^2 \quad (3)$$

Cross-linked caseins are initially in a relaxed state and do not bind water, so that the reservoir volume II has the value 0 at the beginning. Due to the loosening of casein–casein bonds or stretching, water binding occurs, and consequently, volume II increases (see the blue curve of the parallel model (I+II) in **Figure 2**). The corresponding rate of volume change for volume II depends on the swelling rate (Rate II) and a deswelling rate (Rate

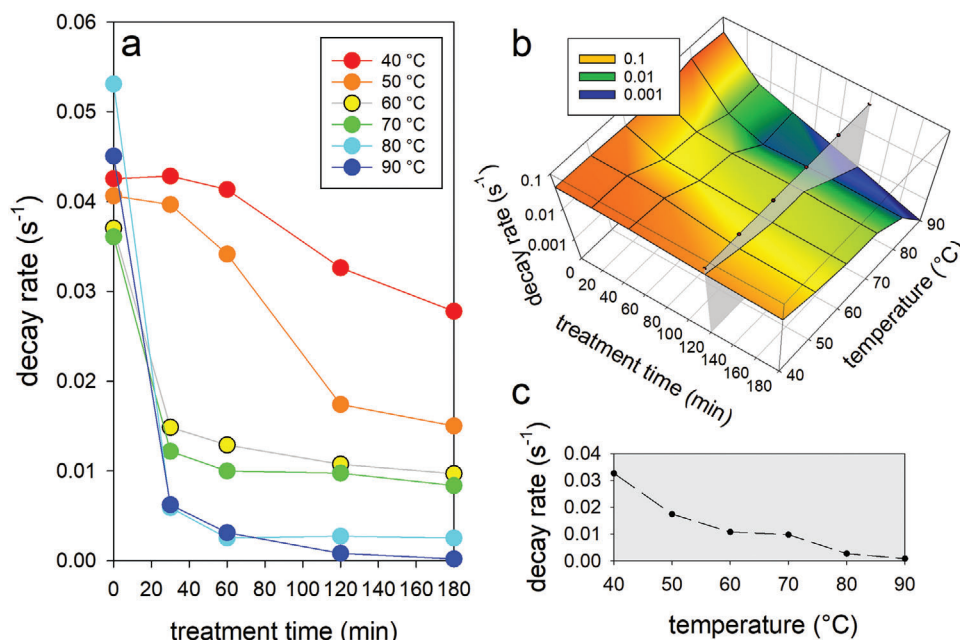


Figure 3. Decay rates of CMPs obtained by fitting SDS decomposition kinetics with a single-exponential function versus treatment time for different temperatures a) and hypersurface of log disintegration rate as a function of treatment time and temperature b). The data points were connected by straight line segments for better visualization.

II*) to simulate the expansion and recovery to the equilibrium state of the network of linked caseins. While the swelling rate is a function of both the rate coefficient II (RC II) activated at time II and the total volume, the deswelling rate depends on the volume II and the rate coefficient RC II* activated at time II*

$$\frac{d \text{volume II}}{dt} = \text{RCII} \cdot \sigma_t^{\text{II}} \cdot \text{totale volume}_t - \text{RCI I}^* \cdot \sigma_t^{\text{II}*} \cdot \text{volume II}_t \quad (4)$$

The total volume of CMPs is then obtained by adding the contributions of volumes I and II.

The system of underlying differential equations for the sequential and parallel model was solved using the Euler integration method with a simulation time step of 0.25 s. Projected particle areas were calculated from the simulated volume profiles using the spherical approximation, which is a good approximation for CMPs for the entire swelling process.^[49]

3. Results and Discussion

The CMPs were heat-treated for different times (0–180 min) and temperatures (40–90 °C) after their preparation according to the process shown in Figure 1. We investigated the effect of post-treatment on the stability and swelling behavior of the CMPs using turbidity measurements in a photometer and swelling experiments in microfluidic sieve cells, both at 20 °C. First, we tested the stability of all post-treated CMPs against SDS using absorbance measurements at 600 nm. Previous studies have shown that CMPs completely decompose after adding SDS, indicating that they are mainly stabilized by hydrophobic interactions.^[32] We used this method to investigate the influence of treatment

temperature and time on the interconnectivity of CMPs. Two decomposition curves were measured from each heat-treated CMPs sample immediately after SDS was added. For all conditions studied, the turbidity measurements showed simple decay curves, which could be fitted with a simple exponential function and characterized by a single decay rate (see the Supporting information, Figure S1). **Figure 3a** shows the decay rates obtained as a function of treatment time for different temperatures. The reference values for the disintegration rates of untreated samples vary between 0.035 and 0.055 s⁻¹ and correspond to the data in Figure 3a at 0 min treatment time.

In general, the decay rates decrease with increasing treatment time and temperature. Thus, for the parameter ranges selected here, CMPs become more stable the higher the treatment temperature and the longer the treatment time is. Figure 3a shows that the rates at temperatures between 60 and 90 °C decrease strongly within the first 60 min, and hardly change thereafter. Interestingly, almost identical final values are reached after 180 min of treatment at T = 80 and 90 °C and T = 60 and 70 °C, respectively. In contrast, major changes in the rates occur only after treatment times > 60 min at temperatures between 40 and 50 °C. The data points connected by straight line segments indicate that the rates in this temperature range decrease sigmoidally, while they tend to decrease exponentially at higher temperatures. The sigmoidal decrease at T = 40 and 50 °C could occur due to a cooperative, temperature-dependent structural transition necessary for the internal gel network of CMPs to compact into a more stable structure. While this cooperative transition takes up to 60 min at moderate temperatures, it occurs within a few minutes in the 60–90 °C temperature range and, therefore, may not have been resolved here due to the temporal resolution of our experiment. As a result, we only observe an exponential decrease in

decay rates due to the transition to the stable, internal network structure. To get an overview of the different stability ranges of the entire data set, we have also plotted the log decomposition rate as a hypersurface versus disintegration time and treatment temperature in Figure 3b. The logarithmic representation was chosen to highlight the stepwise variation of rates at medium to high treatment times and temperatures. The corresponding logarithmic color scale highlights differences in the range of high stability or low decay rates. Based on the 3d plot, three stability ranges can be identified, with the most stable (blue coloring) with decay rates of $< 0.01 \text{ s}^{-1}$ being reached only after a heat treatment of $T = 80^\circ\text{C}$ and treatment times exceeding 60 min. In contrast, medium stabilities with rates in the range of 0.01 s^{-1} (yellow coloration) are achieved by temperature treatment between $T = 50\text{--}70^\circ\text{C}$ for more than 40 min. It can be clearly seen that in this range, the lower the treatment temperature, the more time is required for stabilization, and vice versa. The same applies to the range of low stabilities with rates around 0.1 s^{-1} (red coloring). Correspondingly fast decays of CMPs are obtained only for very short treatment times or temperatures of $T < 60^\circ\text{C}$. In the curves in Figure 3a, the three decay regimes are covered only at temperatures of $T = 80$ and 90°C . The intermediate state can probably not be displayed due to a lack of time resolution. However, if the 3d hyperplane in Figure 3b is intersected at a constant treatment time of 120 min (the gray plane in Figure 3b), a step-like progression can be seen in the corresponding 2d plot in Figure 3c. The results show that thermal post-treatment causes stabilization of the CMPs, which is stronger at higher temperatures and longer treatment times. Furthermore, a region of intermediate stability of the decay rate hyperplane indicates a stable intermediate state resulting in a change of the decomposition mechanism.

It has been reported that weakening of hydrophobic interactions in polymer gels by urea leads to swelling due to hydrophobic hydration.^[50,51] We performed swelling experiments on individual CMPs at pH 11 and $T = 20^\circ\text{C}$ to investigate further the changes in the decomposition mechanism and water-binding behavior caused by previous temperature post-treatment. To compare with Figure 3c, we heat-treated the CMPs for 120 min each at temperatures between $T = 40\text{--}90^\circ\text{C}$ after their preparation. After that, the increase in particle area was measured for two CMPs each after the pH value was increased from pH 6.5 to pH 11 by buffer exchange in the swelling cell. Figure 4 shows the averaged and normalized data of the swelling curves determined in this way for all measured temperatures. The CMPs swell after treatment up to $T = 60^\circ\text{C}$ in a two-step process and finally decompose after their area has reached at least five times the initial size. In contrast, CMPs swell only to a limited extent after a temperature treatment between $70\text{--}90^\circ\text{C}$ and do not decompose even after 2 h in the swelling medium. It is noticeable that the swelling curves of CMPs treated in the medium temperature range ($60\text{--}70^\circ\text{C}$) behave somewhat differently during swelling. For CMPs treated at 60°C , the swelling process starts with the longest delay only after about 12 min, and an exceptionally large degree of swelling (10 times the initial swelling area) is achieved. Swelling curves of CMPs with 70°C treatment temperature, in contrast to 80 and 90°C , show no overshooting after about 12 min and reach higher equilibrium swelling values after a longer time (30 min).

Figure 5 shows the swelling curves of individual CMPs and simulations for the control sample held at 20°C and for CMPs

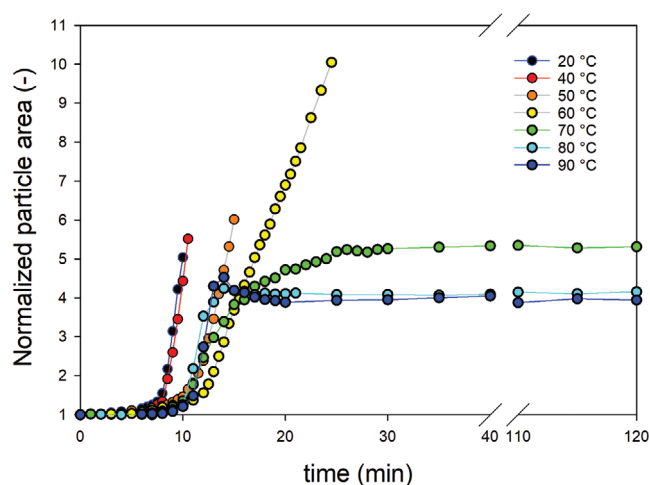


Figure 4. Averaged and normalized swelling kinetics at pH 11 and $T = 20^\circ\text{C}$ of CMPs that were previously heat-treated for 120 min at different temperatures.

post-treated at $T = 40$ and 50°C , respectively. In contrast to Figure 4, the change in absolute particle area is shown as a function of time from only one of the two measured swelling curves in each case. The different starting values result from the different initial sizes of the investigated CMPs. All swelling curves show the typical two-step course and can be best described with the sequential swelling model.^[33] While the first swelling step starts at the same time for all samples after about 200 s, the second swelling step for CMPs starts later for the samples with higher post-treatment temperatures.

For a closer look, the rates of the two swelling steps obtained from the simulation are plotted above their characteristic start times in a double-logarithmic plot in Figure 6. The values of the rates and the corresponding characteristic times are in a range that has been determined in previous measurements for CMPs swelling kinetics at pH 11.^[33] No differences can be detected between the three samples for the values of the first swelling step, as they are within their error limits for both the rate RC Ia and the characteristic time. In contrast, differences between the heat-treated samples can be detected for the rate coefficient of the second swelling process, RC Ib. While there are no differences between CMPs post-treated at 40°C and control, post-treating the CMPs at 50°C results in a delayed start time and a significantly lower rate. According to our model, the volume of the granular microstructure of the CMPs increases during the first swelling step. The second swelling step loosens the interconnecting contacts between the microstructures eventually leading to the complete disintegration of the CMPs.^[31] Our simulation results show that post-treatment at moderate temperatures does not affect the expansion of the internal microstructure elements but the stabilizing interactions between them. The delayed start time and reduced speed of the second swelling process indicate that the contacts between the microstructure are improved after temperature treatment at 50°C . The interaction between caseins is mainly a result of hydrophobic as well as electrostatic contacts between calcium and phosphate groups.^[14] Based on the higher SDS stability and the observed temperature dependence of the swelling curves,

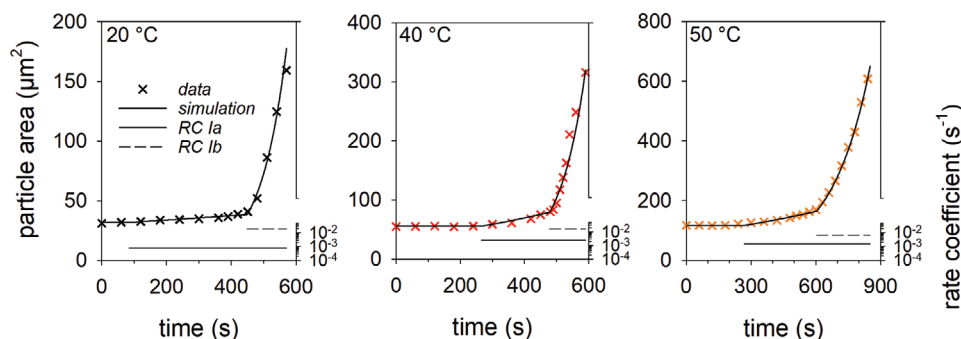


Figure 5. Swelling curves (pH 11 and $T = 20\text{ }^{\circ}\text{C}$) and simulations with the sequential dynamic model of single CMPs, untreated and after 120 min post-treatment at $T = 40$ and $50\text{ }^{\circ}\text{C}$. The effective ranges of the rate coefficients for the two swelling steps, RC Ia and RC Ib, are shown in the lower part of the figure.

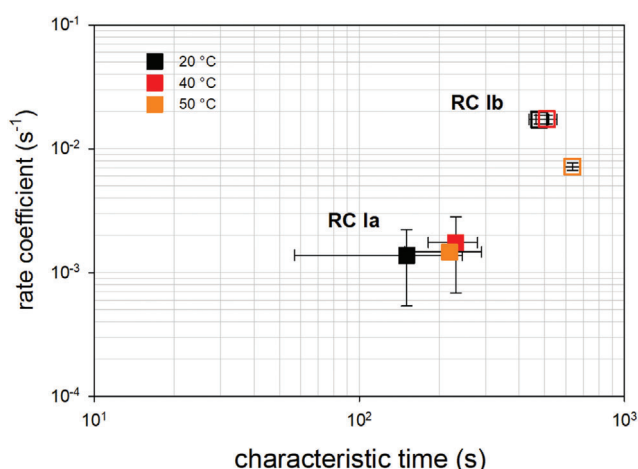


Figure 6. Rate coefficients as a function of the characteristic times from the simulations of the swelling kinetics with the sequential dynamic model for the control sample at $T = 20\text{ }^{\circ}\text{C}$ and for the CMPs post-treated for 120 min at $T = 40$ and $50\text{ }^{\circ}\text{C}$. The data from the first swelling step are shown as closed symbols and those from the second swelling step as open symbols.

it can be assumed that new hydrophobic contacts are formed during temperature treatment, which persists after cooling to $20\text{ }^{\circ}\text{C}$ and reinforce the structure. Moreover, our recent results have shown that calcium chelator citrate does not affect the rate of the second swelling step.^[36] This suggests that hydrophobic interactions, rather than calcium-mediated electrostatic contacts, actually exist between the casein interfaces of the microstructure and that they are responsible for the effect.

Post-treatment for 120 min at $T = 60$ and $70\text{ }^{\circ}\text{C}$ resulted in even more stable CMPs, with the swelling process not leading to immediate decay, but converging to a maximum equilibrium swelling value. A more detailed investigation revealed additional features in the swelling kinetics (see **Figure 7**). Within the red-marked time range, up to ≈ 700 s of the swelling kinetics for $T = 60$ and $70\text{ }^{\circ}\text{C}$, a two-step swelling process still takes place. However, further swelling steps become visible for longer times, which cannot be described by the sequential swelling model alone. Instead, we now use the parallel swelling model (I + II) in **Figure 2**, which we used in a similar form to describe the

swelling kinetics of CMPs treated with TGase.^[37] A new feature is that the two-step swelling process can be resolved for temperature-treated CMPs at the beginning, which was not possible after TGase treatment because, in this case the neighboring interfaces of the microstructure were probably covalently cross-linked with each other, so the second swelling process did not occur.

The exact partition of the simulated swelling kinetics (black line) into the parallel swelling processes is shown on the right side in **Figure 7**. The time course of volume I (red line) corresponds to the sequential swelling of the caseins, which was indirectly influenced by the temperature treatment. Volume II (blue line), on the other hand, can be assigned to the casein portion stabilized due to the temperature post-treatment. The new bonds inserted by temperature treatment at $T = 60\text{ }^{\circ}\text{C}$ are not yet able to stabilize the overall structure and can only slow down the decomposition. As a result of the stepwise expansion of volume I, volume II also expands very strongly within 200 s from about 700 s onward and at a smaller rate from about 900 s onward. In contrast, after treatment at $T = 70\text{ }^{\circ}\text{C}$ for 120 min, the newly and irreversibly formed bonds are already so strong that the corresponding kinetics for volume II reaches an equilibrium end value at times > 3000 s. Furthermore, overshooting occurs after about 1500 s, which we had already considered in the analysis of CMPs covalently cross-linked by TGase.^[37] According to our model, cross-linked casein components elastic network is overstretched during the expansion of the uncross-linked caseins. Similar to a stretched spring, this causes a restoring force that brings the system back to its equilibrium state. As a result, water is squeezed out and the volume or cross-sectional area of the CMPs becomes smaller again. Overshooting in the swelling kinetics was also observed in other polymer systems and explained by the ionic contribution to the free enthalpy.^[38,39,40] Since the effect increases with increasing treatment time with TGases or temperature in this study, we assume that overshooting can rather be attributed to the elastic contributions due to the newly formed bonds between the caseins.^[37] After post-treatment temperatures above $T = 80\text{ }^{\circ}\text{C}$, the characteristic behavior of the newly cross-linked casein fraction increasingly dominates the simulated swelling kinetics via model volume II (see blue curve in **Figure 8**, right). Also, in the measured data (**Figure 8**, left), the overshooting effect is now clearly visible at $T = 80\text{ }^{\circ}\text{C}$ and further intensifies at $T = 90\text{ }^{\circ}\text{C}$.

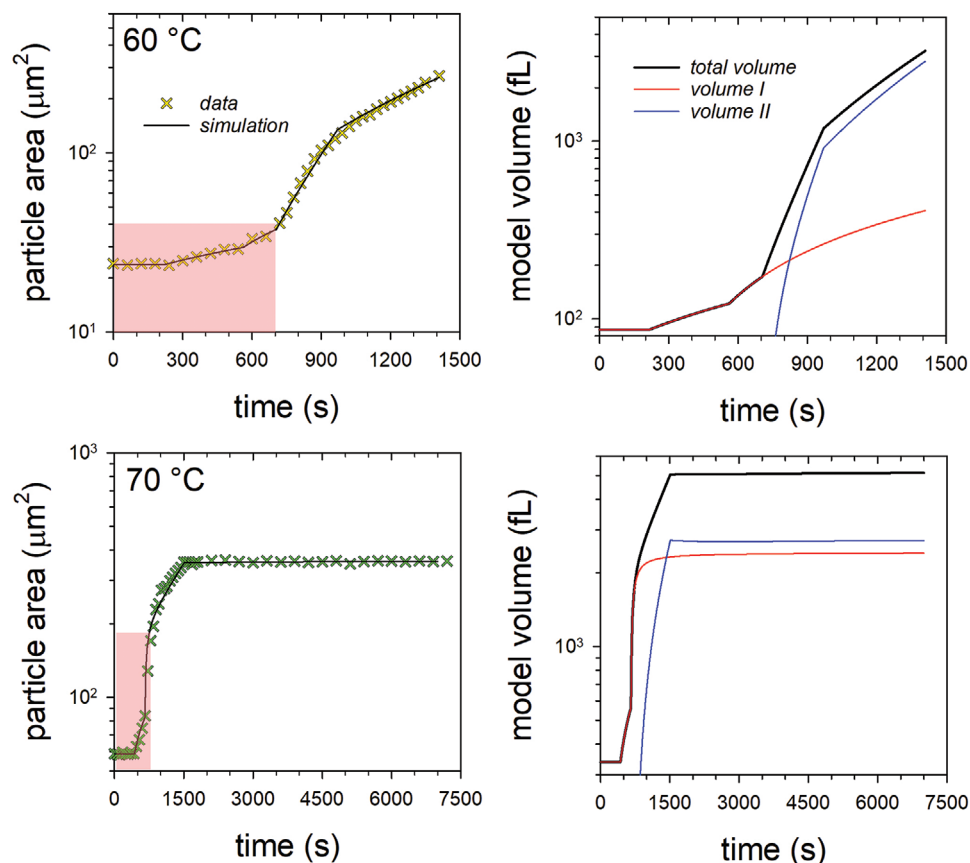


Figure 7. Swelling data at pH 11 and $T = 20\text{ }^{\circ}\text{C}$ (crosses) and corresponding simulations with the parallel dynamic model (solid line) of single CMPs with 120 min post-treatment at $T = 60$ and $70\text{ }^{\circ}\text{C}$. The simulated total volume, which is composed of volume I for the noncross-linked and volume II for the additionally cross-linked caseins, is shown on the right.

Figure 9 shows the mean values of the parameters of the parallel swelling model for all treatment temperatures. Each mean value and the plotted error range are based on two swelling kinetics per condition. As **Figure 9a** shows, all swelling steps of the noncross-linked casein fraction occur between 100 and 1000 s and thus lie in the time range generally determined for swelling kinetics of CMPs at pH 11.^[33,37,49] The values of the rates are several orders of magnitude smaller than those of the untreated CMPs or the CMPs post-treated at $T = 30$ and $40\text{ }^{\circ}\text{C}$ (compare **Figure 6**) and cannot be directly compared. The reason for this is the maximum degree of crosslinking V_{∞} considered in the parallel swelling model, which limits swelling and results in significantly smaller values. The rates of the second swelling process (rate Ib*, open symbols in **Figure 9a**) are larger than those of rate Ia* (first swelling step) for all treatment temperatures, which we always observed for untreated CMPs.^[33,49] Moreover, the rates of both swelling steps for CMPs with $T = 80$ and $90\text{ }^{\circ}\text{C}$ post-treatment temperatures are higher than those obtained at temperatures of $T = 60$ and $70\text{ }^{\circ}\text{C}$, respectively. This effect can also be seen directly in the normalized swelling kinetics in **Figure 4**, where the swelling curves of 60 and $70\text{ }^{\circ}\text{C}$ rise the lowest before rising steeply again at $T = 80$ and $90\text{ }^{\circ}\text{C}$. About the reason for this can only be speculated at present. However, the sigmoidal course of the SDS decomposition rates as a function of the treatment temperature (**Figure 3c**) indicates a cooperative,

internal restructuring process of the CMPs as a result of the temperature post-treatment. A stable but rather unstructured intermediate state is reached only when a certain fraction of caseins are relinked. This is the case, for example, after 120 min of temperature treatment in the temperature range of $60\text{ }^{\circ}\text{C}$. The corresponding volume II within the parallel model (the blue curve, **Figure 7** above) continues to expand as a result of the swelling process and is not yet able to stabilize the overall structure of the CMPs. The casein fraction that crosslinks at $T = 60\text{ }^{\circ}\text{C}$ probably densifies the original network structure of the CMPs, so the swelling process is strongly delayed at $T = 20\text{ }^{\circ}\text{C}$ and pH 11. Due to the new casein–casein contacts, however, the CMPs treated in this way do not decompose until their microscopically visible particle areas reach ten times their initial value. After post-treatments with even higher temperatures ($T = 80$ and $90\text{ }^{\circ}\text{C}$), the internal restructuring is possibly finally completed, again resulting in a rather sponge-like structure consisting of casein-rich and solvent-rich compartments. A network structure stabilized by hydrophobic contacts between caseins could explain the increased stability of CMPs treated in this way. The void structure formed by the network would again exhibit a high water binding capacity, which could explain the higher swelling rates of these CMPs. The values of rate Ia* and rate Ib* can be compared with the rate of the noncross-linked casein fraction of CMPs treated with TGase from earlier measurements, which were also analyzed with the

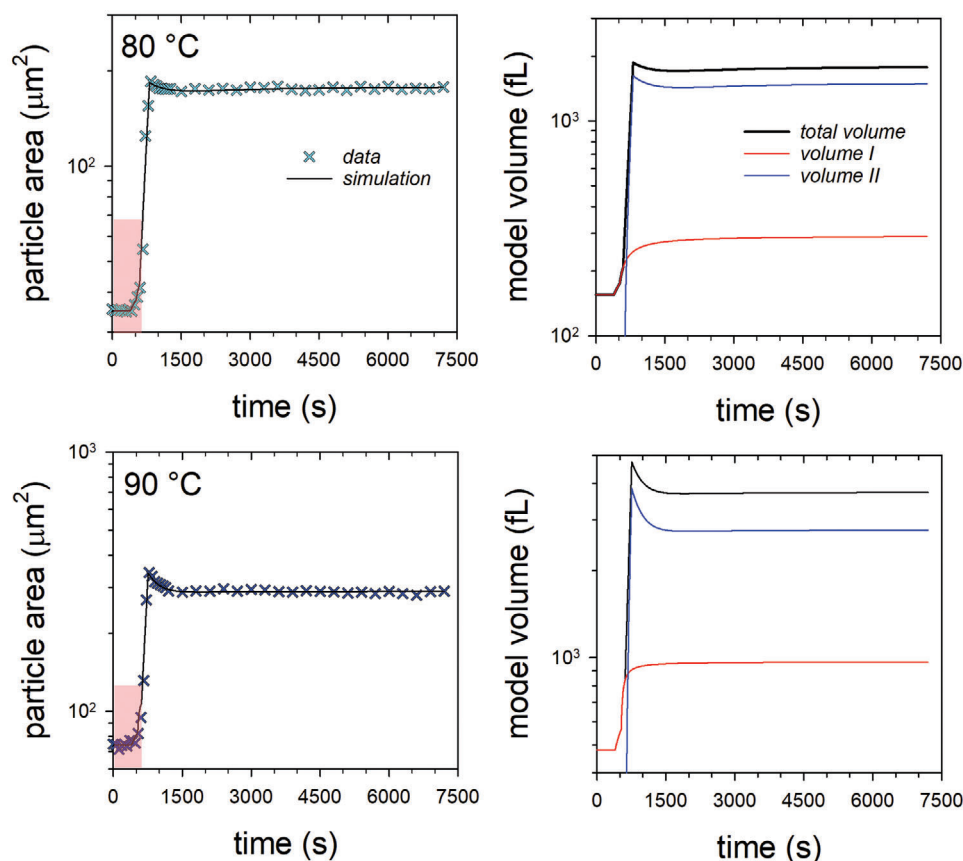


Figure 8. Swelling data at pH 11 and $T = 20\text{ }^{\circ}\text{C}$ (crosses) and corresponding simulations with the parallel dynamic model (solid line) of single CMPs with 120 min post-treatment at $T = 80$ and $90\text{ }^{\circ}\text{C}$. The simulated total volume, which is composed of volume I for the noncross-linked and volume II for the additionally cross-linked caseins, is shown on the right.

parallel model. Based on similar values, it can be concluded that a 120 min temperature post-treatment at $T = 80$ or $90\text{ }^{\circ}\text{C}$ results in a similar effect on the swelling rates of the noncross-linked casein fraction at pH 11 as a 1 h TGase post-treatment under conditions as described in Gebhardt et al.^[37] In contrast, even an increase in swelling could be achieved by this temperature treatment for the elastically linked casein portion. The corresponding values for the rates of the swelling and deswelling step (rate II and rate II*) are above 10^{-2} s^{-1} after treatment with $T = 80$ and $90\text{ }^{\circ}\text{C}$ and thus above those determined for the sample treated with TGase. Figure 9b again shows that both rates for CMPs at $T = 80$ and $90\text{ }^{\circ}\text{C}$ are larger than those for CMPs post-treated at $T = 60$ and $70\text{ }^{\circ}\text{C}$. This is firstly in contradiction to the assumption that at higher temperatures more bonds are formed between the caseins, making their swelling more difficult. On the other hand, the rates of cross-linked caseins in Figure 9b are strongly coupled with those of uncross-linked caseins in Figure 9a. Since the noncross-linked caseins swell fastest at $T = 80$ and $90\text{ }^{\circ}\text{C}$, the cross-linked caseins are also stretched faster, resulting in higher rates. Post-treatment at higher temperatures also leads to smaller equilibrium swelling values (see the normalized swelling curves in Figure 4). As CMPs with different initial sizes were investigated for the temperature-dependent swelling kinetics, we related their maximum equilibrium swelling values V_{∞} to the corresponding initial volumes I and plotted the resulting ratio as a function of the treatment tem-

perature in Figure 9c. It can be seen in the semilogarithmic plot that the relative equilibrium swelling value drops sharply from 40 times at $T = 60\text{ }^{\circ}\text{C}$ to only twice the initial volume at $T = 80\text{ }^{\circ}\text{C}$ and does not change further after a further temperature increase to $90\text{ }^{\circ}\text{C}$. A decrease in equilibrium swelling values can be attributed to an increase in gel crosslinking, but this is also accompanied by a decrease in swelling rate.^[22,23] This supports our assumption that an increasing irreversible fraction of newly cross-linked caseins are formed during the temperature post-treatment, which, however, also restructures the CMPs. New casein–casein contacts delay the swelling process at medium temperatures (see smaller values RC II for $T = 60$ and $70\text{ }^{\circ}\text{C}$ in Figure 9b). However, these are not yet strong enough after $60\text{ }^{\circ}\text{C}$ treatment, so the decomposition cannot be prevented and comparatively high swelling values are achieved. Only after a 120 min post-treatment at $T = 70\text{ }^{\circ}\text{C}$ the CMPs no longer decompose during swelling and stabilize at an equilibrium swelling value. At post-treatment temperatures of $80\text{ }^{\circ}\text{C}$ and higher, additional formed contacts further reduce the equilibrium swelling value. At the same time, the swelling rates (RC Ia* and RC Ib* as well as RC II* and RC II*) increase again, which can only be explained by an internal restructuring of the CMPs toward a rapid swelling and stable elastic network structure. This restructuring could be a consequence of the increased mobility of caseins, which, for example, melts the rigid structure of casein micelles in the temperature range above $70\text{ }^{\circ}\text{C}$.^[43] The

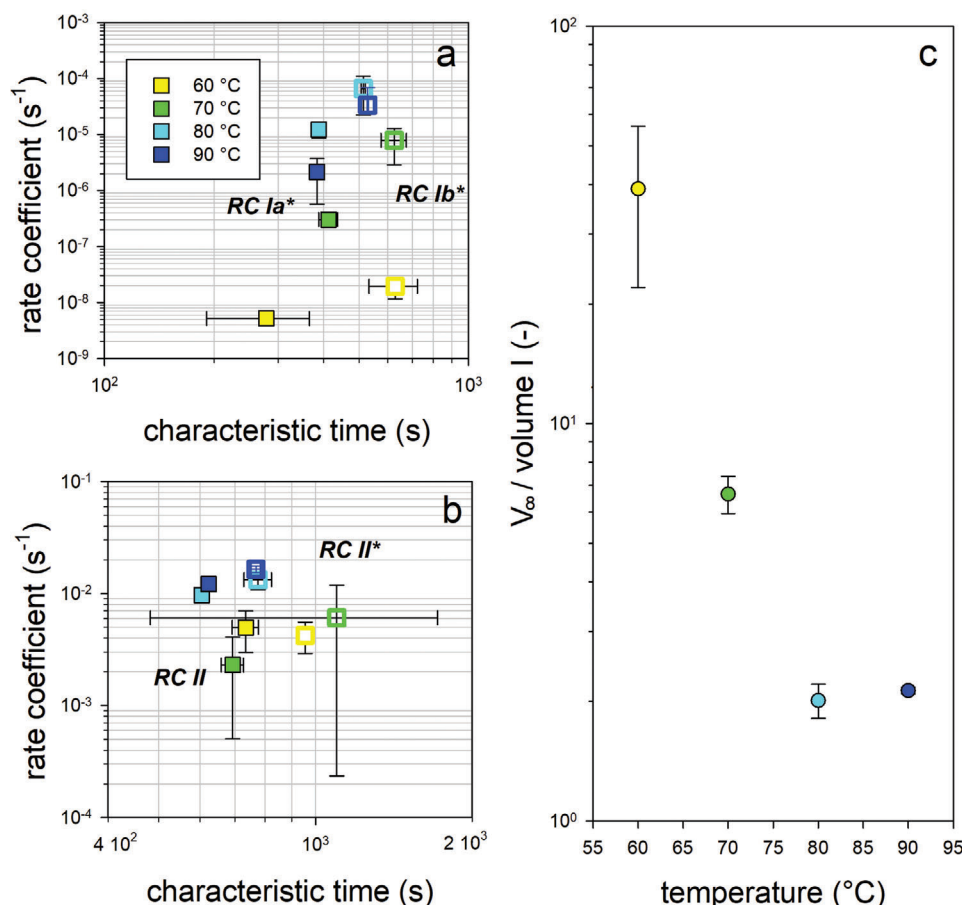


Figure 9. Parameter values of the parallel swelling model used to describe the swelling kinetics of the CMPs post-treated for 120 min with temperatures between $T = 60$ and 90 °C. As a function of the characteristic times, the rates of noncross-linked casein fraction are shown in a) and cross-linked casein fraction in b), while the maximum equilibrium degree of swelling achieved is shown as a function of treatment temperature in c).

restructuring of the internal structure is also supported by the observed decay rates in Figure 3c, which suggest at least two stable structural states of the CMPs, as a result of temperature post-treatment.

4. Conclusion

Temperature post-treatment is necessary to ensure the microbiological safety of polymer systems, but structural and functional changes, especially in proteins, should be considered. SDS decay rates and swelling curves indicate a complex, temperature-induced restructuring process of the CMPs that proceeds via an intermediate state. CMPs that were post-treated for at least 120 min at temperatures of 40 and 50 °C decayed comparatively quickly after adding SDS but more slowly the higher the treatment temperature was. Since the swelling curves in this temperature range can still be analyzed with the standard sequential model, major structural changes can be excluded. For post-treatment temperatures between 50 and 90 °C, the SDS stability of the CMPs increases over an intermediate state between 60 and 70 °C. In this temperature range, the swelling steps are delayed and the swelling rates reduced, which we attribute to a relatively homogeneous internal structure of the intermedi-

ate state that makes water penetration more difficult. Further changes in the swelling curves can only be simulated with an extended parallel modeling approach, which has already been successfully used to describe the swelling of CMPs with subsequently inserted cross-links.^[37] These new characteristic features in the swelling curves can thus be attributed to structure-stabilizing contacts resulting from the heat treatment. At temperatures of 60 °C and above, the swelling curves now converge to equilibrium swelling values, which become smaller with increasing temperature, as shown by our model simulations. The lowest equilibrium swelling values are obtained after post-treatment temperatures of $T > 80$ °C for CMPs, whose SDS stability is further enhanced. Contrary to the trend, CMPs treated in this way now swell comparatively rapidly, so we assume an internal structural transformation to a stable network structure at these high temperatures, which irreversibly persists after the post-treatment process. The newly observed elastic network structure of the temperature-treated CMPs should be characterized nanomechanically in the future, as has already been done for TGase-treated casein nanogel particles.^[52] The internal structures of CMPs can be visualized in future studies, e.g., with confocal fluorescence microscopy, to better understand the swelling and decay process of CMPs in view of their potential application as carriers

for bioactive compounds with immediate or controlled release function.^[40]

Supporting Information

Supporting Information is available from the Wiley Online Library or from the author.

Acknowledgements

The authors are grateful to Calvin Hohn for experimental help and Jann Schulte for helpful discussions. The swelling cells were thankfully 3D printed by AVT.CVT.

Open access funding enabled and organized by Projekt DEAL.

Conflict of Interest

The authors declare no conflict of interest.

Data Availability Statement

The data that support the findings of this study are available from the corresponding author upon reasonable request.

Keywords

casein microparticles, dynamic modeling, swelling, thermal processing

Received: November 24, 2022

Revised: January 19, 2023

Published online:

- [1] D. G. Dalgleish, *Soft Matter* **2011**, 7, 2265.
- [2] X. Wang, Z. Zhao, *J. Food Eng.* **2022**, 333, 111138.
- [3] U. Sadiq, H. Gill, J. Chandrapala, *Foods* **2021**, 10, 1965.
- [4] L. Chen, J. Wei, M. An, L. Zhang, S. Lin, G. Shu, Z. Yuan, J. Lin, G. Peng, X. Liang, L. Yin, W. Zhang, L. Zhao, H. Fu, *Colloids Surf., B* **2020**, 195, 111221.
- [5] M. Bar-Zeev, D. Kelmansky, Y. G. Assaraf, Y. D. Livney, *Eur. J. Pharm. Biopharm.* **2018**, 133, 240.
- [6] T. K. Głab, J. Boratyński, *Top. Curr. Chem.* **2017**, 375, 71.
- [7] B. P. Ismail, L. Senaratne-Lenagala, A. Stube, A. Brackenridge, *Animal Front.* **2020**, 10, 53.
- [8] A. Bernhardt, M. Wehr, B. Paul, T. Hochmuth, M. Schumacher, K. Schütz, M. Gelinsky, *PLoS One* **2015**, 10, e0129205.
- [9] S. G. Anema, *Int. Dairy J.* **2021**, 122, 105136.
- [10] N. Peelman, P. Ragaert, K. Ragaert, B. De Meulenaer, F. Devlieghere, L. Cardon, *J. Appl. Polym. Sci.* **2015**, 132, n/a.
- [11] C. Holt, L. Sawyer, *J. Chem. Soc. Faraday Trans.* **1993**, 89, 2683.
- [12] C. Broyard, F. Gaucheron, *Dairy Sci. Technol.* **2015**, 95, 831.
- [13] C. Holt, *Eur. Biophys. J.* **2021**, 50, 847.
- [14] D. S. Horne, *Int. Dairy J.* **1998**, 8, 171.
- [15] V. I. Uricanu, M. H. G. Duits, J. Mellema, *Langmuir* **2004**, 20, 5079.
- [16] R. Gebhardt, N. Takeda, U. Kulozik, W. Doster, *J. Phys. Chem. B* **2011**, 115, 2349.
- [17] Y. Liu, R. Guo, *J. Colloid Interface Sci.* **2007**, 315, 685.
- [18] C. G. De Kruif, *Int. Dairy J.* **1999**, 9, 183.
- [19] M. Quesada-Pérez, J. A. Maroto-Centeno, J. Forcada, R. Hidalgo-Alvarez, *Soft Matter* **2011**, 7, 10536.
- [20] C. G. (K.) De Kruif, S. G. Anema, C. Zhu, P. Havea, C. Coker, *Food Hydrocoll.* **2015**, 44, 372.
- [21] K. Haraguchi, J. Ning, G. Li, *Eur. Polym. J.* **2015**, 68, 630.
- [22] D. K. Aktaş, G. A. Evingür, Ö. Pekcan, *Adv. Polym. Technol.* **2009**, 28, 215.
- [23] A. S. Kipcak, O. Ismail, I. Doymaz, S. Piskin, *J. Chem.* **2014**, 2014, 281063.
- [24] A. Bouchoux, G. Gésan-Guizieu, J. Pérez, B. Cabane, *Biophys. J.* **2010**, 99, 3754.
- [25] D. J. McMahon, B. S. Oommen, *J. Dairy Sci.* **2008**, 91, 1709.
- [26] T. Huppertz, I. Gazi, H. Luyten, H. Nieuwenhuijse, A. Alting, E. Schokker, *Int. Dairy J.* **2017**, 74, 1.
- [27] D. G. Dalgleish, M. Corredig, *Annu. Rev. Food Sci. Technol.* **2012**, 3, 449.
- [28] T. Nicolai, C. Chassenieux, *Food Hydrocoll.* **2021**, 118, 106755.
- [29] Y. Zhuang, J. Sterr, U. Kulozik, R. Gebhardt, *Int. J. Biol. Macromol.* **2015**, 74, 44.
- [30] Y. Zhuang, J. Sterr, A. Schulte, U. Kulozik, R. Gebhardt, *Recent Adv. Food Sci.* **2016**, 11, 332.
- [31] J. Schulte, M. Stöckermann, S. Thill, R. Gebhardt, *Int. Dairy J.* **2020**, 105, 104692.
- [32] J. Schulte, T. Pütz, R. Gebhardt, *Int. Dairy J.* **2022**, 133, 105422.
- [33] J. Schulte, M. Stöckermann, R. Gebhardt, *Food Hydrocoll.* **2020**, 105, 105741.
- [34] R. Gebhardt, E. Pechkova, C. Riekel, C. Nicolini, *Biophys. J.* **2010**, 99, 1262.
- [35] B. B. Eedara, I. G. Tucker, S. C. Das, *Sci. Rep.* **2019**, 9, 18522.
- [36] M. d. Asaduzzaman, T. Pütz, R. Gebhardt, *Sci. Rep.* **2022**, 12, 1840.
- [37] R. Gebhardt, S. Khanna, J. Schulte, M. d. Asaduzzaman, *Int. J. Mol. Sci.* **2022**, 23, 11837.
- [38] H. Takeno, Y. Kimura, W. Nakamura, *Gels* **2017**, 3, 10.
- [39] H.-Y. Ren, M. Zhu, K. Haraguchi, *Macromolecules* **2011**, 44, 8516.
- [40] S. Thill, T. Schmidt, S. Jana, D. Wöll, R. Gebhardt, *Macromol. Mater. Eng.* **2022**, 307, 2200272.
- [41] D. S. Horne, *Curr. Opin. Colloid Interface Sci.* **2006**, 11, 148.
- [42] C. Broyard, F. Gaucheron, *Dairy Sci. Technol.* **2015**, 95, 831.
- [43] H. S. Rollema, J. A. Brinkhuis, H. J. Vreeman, *Neth. Milk Dairy J.* **1988**, 42, 233.
- [44] M. Asaduzzaman, M. S. Mahomud, M. E. Haque, *Int. J. Food Sci.* **2021**, 2021, 5569917.
- [45] J. Dumpler, I. Kieferle, H. Wohlschläger, U. Kulozik, *Int. Dairy J.* **2017**, 68, 60.
- [46] C. G. De Kruif, R. Tuinier, *Food Hydrocoll.* **2001**, 15, 555.
- [47] A. Marozienne, *Food Hydrocoll.* **2000**, 14, 391.
- [48] H. Schott, *J. Macromol. Sci., Part B: Phys.* **1992**, 31, <https://doi.org/10.1080/00222349208215453>.
- [49] J. Schulte, T. Pütz, R. Gebhardt, *Food Hydrocoll. Health* **2021**, 1, 100014.
- [50] T. Huppertz, M. A. Smiddy, C. G. De Kruif, *Biomacromolecules* **2007**, 8, 1300.
- [51] K. Miyamoto, M. Tokita, T. Komai, *Protein Pept. Lett.* **2001**, 8, 231.
- [52] A. Bahri, M. Martin, C. Gergely, S. Marchesseau, D. Chevalier-Lucia, *Food Hydrocoll.* **2018**, 83, 53.